Deterministic and Controllable Photonic Scattering Media via Direct Laser Writing

Evangelos Marakis, Ravitej Uppu, Maryna L. Meretska, Klaas-Jan Gorter, Willem L. Vos, and Pepijn W. H. Pinkse*

Photonic scattering materials, such as biological tissue and white paper, are made of randomly positioned nanoscale inhomogeneities in refractive index that lead to multiple scattering of light. Typically these materials, both naturally occurring or man-made, are formed through self assembly of the scattering inhomogeneities, making it extremely challenging to know the exact positions of these inhomogeneities, let alone control those. Here, the nanofabrication of photonic multiple-scattering media using direct laser writing with a deterministic design is reported on. These deterministic multiple-scattering media consist of submicron-thick polymer nanorods that are randomly oriented within a cubic volume. The total transmission of light is studied as a function of the number of rods and of the sample thickness to extract the scattering and transport mean free paths using radiative transfer theory. Such ability to fabricate photonic multiple-scattering media with deterministic and controllable properties opens up a myriad of opportunities for fundamental studies of light scattering, in particular, in the multiple-scattering regime and with strong anisotropy and for new applications in solid-state lighting and photovoltaics.

1. Introduction

The scattering of light is a familiar physical process that is abundant in everyday life and in nature; manifestations of scattering are the opacity of white paper, of clouds, and of biological tissue.[1–16] Light scattering occurs at any interface

E. Marakis, Dr. R. Uppu,[+] Dr. M. L. Meretska,[++] K.-J. Gorter,
Prof. W. L. Vos, Prof. P. W. H. Pinkse
Complex Photonic Systems (COPS)
MESA+ Institute for Nanotechnology
University of Twente
PO Box 217, Enschede 7500 AE, The Netherlands
E-mail: p.w.h.pinkse@utwente.nl

[+]Present address: Center for Hybrid Quantum Networks (Hy-Q), Niels Bohr Institute, University of Copenhagen, Blegdamsvej 17, Copenhagen 2100, Denmark

[++]Present address: Harvard John A. Paulson School of Engineering and Applied Sciences, Harvard University, Cambridge, MA 02138, USA

between different materials and causes a part of the light to deviate from its original path. A sufficiently thick medium with a high density of such interfaces acts as a multiple-scattering material. The light transport through and interaction with the scattering medium is characterized by two characteristic length scales: the scattering mean free path ℓ_{sc} and the transport mean free path ℓ_{tr}. The scattering mean free path quantifies the mean distance between subsequent scattering events. The mean distance that the incident light propagates before its direction is scrambled is the transport mean free path ℓ_{tr}. Scattering media with $L > \ell_{tr} > \lambda$, where L is its physical thickness and λ is the wavelength of light in the embedding medium, support diffusive transport of light and play an important role in devices such as solar cells and white LEDs. For instance, a thin scattering layer on top of a solar cell increases the absorption of sunlight and hence the cell's efficiency.[14] White LEDs employ a layer of scattering and phosphor particles to control the spectral and spatial distribution of the emission.[13,16] The aforementioned applications of scattering media often require a specific optical thickness, defined as the ratio L/ℓ_{tr}, and a carefully designed angular distribution of light quantified through the scattering anisotropy g.[17] For example, high opacity diffusing media that could benefit white LEDs and thin film solar cells require that the physical thickness L exceeds the scattering mean free path ($L/\ell_{sc} > 1$) for enhanced absorption, while ensuring directional illumination or minimal backscattering, that is, $\ell_{tr} \approx L$. Importantly, such scattering media benefit from physical thickness down to a few µm, necessitating short $\ell_{sc} \approx$ µm. In a non-absorbing scattering medium, g relates the mean free paths as $(1 - g)\ell_{tr} = \ell_{sc}$, hence the LEDs and solar cells require designer scattering media with short ℓ_{sc} and large g.

A large number of scattering media with well-defined scattering properties, covering a broad range of optical thicknesses have been presented in the literature.[18–23] However, the fabrication of those media rely on random processes and only the average values are controlled during fabrication. Knowledge about the internal structure or actually tailoring the internal structure on the microscopic scale would give an entirely new level of control of the scattering properties, for example, by employing the rapidly evolving inverse design techniques.[24,25] However, revealing the microscopic internal structure of

**ADVANCED
SCIENCE NEWS**

www.advancedsciencenews.com

**ADVANCED
OPTICAL
MATERIALS**

www.advopticalmat.de

multiple-scattering media requires careful dissection of the media for sub-micron inspection, thereby destroying the medium in the process. Recent advances in 3D nanofabrication[26–28] has made it feasible to create a scattering medium with a precisely known predetermined internal structure. A priori knowledge of the internal structure makes it ideal for studies of light propagation that are sensitive to microscopic wave interference of light.[29] In the literature, several scattering media with deterministic geometry and scattering properties have been demonstrated using different nanofabrication techniques. Matoba et al.[30] have created a large-volume deterministic scattering medium with laser micromachining,[31,32] but with undefined scattering strength. An alternative nanofabrication technique is direct laser writing (DLW),[27] offering about 1–10 nm material deposition precision and a feature size down to about 100 nm.[26] DLW encompasses many technical variations and definitions.[33–35] In the present work, we focus on DLW employing multiphoton lithography. The physical principle of this type of DLW is multiphoton absorption, which initiates polymerization at a targeted location inside the volume of the photoresist. The advantage of DLW is the freedom to create deterministic and complex 3D geometries. An example of a DLW-nanofabricated photonic structure with complex geometry is the hyperuniform medium fabricated by Haberko et al.[36–38] In the current work, we report on the fabrication of deterministic scattering media that combine both a large anisotropy and a short (few micrometer) scattering mean free path. We measure the transport mean free path of the structures and validate that light scattering in our structures is in the diffusive regime ($L/\ell_{tr} > 1$).

2. Designing a Deterministic Scattering Medium

We realize direct laser-written disordered scattering media as a collection of randomly-oriented polymer rods in a cubic volume. As described in ref. [39], we developed an algorithm based on Jaynes' solution to Bertrand's paradox to ensure an on-average uniform filling of the volume and the random positioning of the rods in the cube with the use of a random number generator. A design example is shown in **Figure 1**b. The randomly intersecting polymer rods run from one facet of the cube to another. Typically, creating mechanically stable structures using DLW requires additional support walls bounding the structure. However, these walls create unwanted light scattering interfaces that complicate the modeling of light transport. Our novel design achieves mechanical stability of the structures without the addition of any support walls, and hence enables direct comparison with theoretical models of light scattering that are necessary for extracting the transport parameters (ℓ_{sc}, ℓ_{tr}, g). The DLW setup is ideally suited to write rods in a successive manner.[40] After generating the coordinates of the rods, the algorithm sorts them such that the rods attached to the substrate are written first, as illustrated in Figure 1a. This creates a stable scaffold to which the other rods are attached to. At the end of the writing process, a rigid structure is created to follow the design model as shown in Figure 1b.

An important parameter that determines the scattering strength of the disordered medium is the filling fraction of
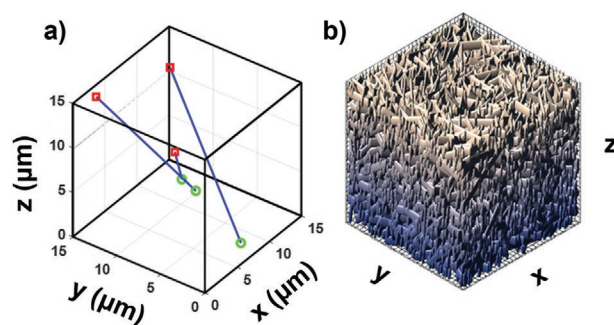
Figure 1. The 3D spatial structure of our deterministic scattering samples. a) First rods are connected to the substrate (green points) in order to make a rigid connected scaffold. The end points lie on another face of the cube (red points). Secondly, rods that are not connected to the substrate are written subsequently. This procedure minimizes drifting of the features during the writing process. b) A rendering of the final model. The features on top have a lighter shading, while the features closer to the substrate are darker.

polymer, which is set by the number of rods written in the cubic volume. Starting from an empty cube, the scattering strength will increase with the number of rods until at some density of rods, the overlapping of the different rods will effectively create a solid block of polymer with a decreasing volume of voids, decreasing the scattering strength of the structure. The desired filling fraction is the one that maximizes light scattering. Creating a free-standing structure requires a minimum number of rods that intersect to form a rigid skeleton that does not collapse under its own weight or under capillary forces. When the number of rods are increased above a certain critical value, the air–polymer surface will decrease, thereby reducing the scattering strength of our structures. **Figure 2** shows the estimated filling fraction and effective refractive index[41] of the structures with increasing number of rods for two fixed structure volumes. The deterministic fabrication of our structures allows us to calculate the filling fraction of the structures,
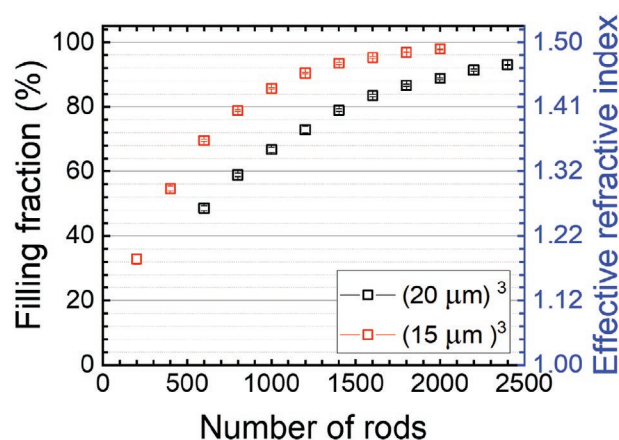
Figure 2. Estimated filling fraction and effective refractive index versus the density of rods over volume. Red markers and line denote how the filling fraction increases with increasing density of rods per volume for structures with volume $(15\ \mu m)^3$, while the black markers show the same trend for cubes of $(20\ \mu m)^3$. The estimation was performed by numerically integrating the volume of the intersecting rods.

**ADVANCED
SCIENCE NEWS**

www.advancedsciencenews.com

**ADVANCED
OPTICAL
MATERIALS**

www.advopticalmat.de

given the knowledge of their design. The fill fraction is numerically estimated by first discretizing the design volume into cubic pixels (voxels) with dimensions of $(20\ nm)^3$ and then binarizing the discretized volume into written and unwritten blocks. The infinitesimal lines in the design are converted to finite thickness by assuming a laser focus of ellipsoidal volume with a diameter of 500 nm and an elongation of 3.5 times the diameter. The digital volumes then are used for the estimation of the effective refractive index numerically.[41] The estimated filling fraction also allows us to estimate the effective refractive index for a wavelength of 633 nm, indicated in Figure 2 by the second ordinate. Hereto we used a simple volume average of the dielectric constants. A higher number of rods is required to reach the same filling fraction in the $(20\ \mu m)^3$ structure in comparison to the $(15\ \mu m)^3$, which highlights isotropic disorder in the structure.

To keep fabrication times acceptable (7 min per structure), we created structures with a lateral size of 15 to 20 μm and a height of up to 20 μm. For structures wider and taller than 20 μm, we suggest the model to be divided into cubes of $(20\ \mu m)^3$ to prevent pyramidal distortions, shadowing effects, and weight deformations.[42,43]

## 3. Results

3.1. Fabrication Quality

We fabricated 693 structures with various thicknesses and filling fractions and employed a scanning electron microscope (SEM) to determine the feature sizes. **Figure 3** shows a qualitative comparison of the surface features in the designed (a, c) and the fabricated structures (b, d) that highlights the similarity. Note that in contrast to the model rendering in (a) and (c), deeper lying lines in the SEM pictures (b) and (d) are not visible. The rod thickness was measured to be 524 ± 60 nm.
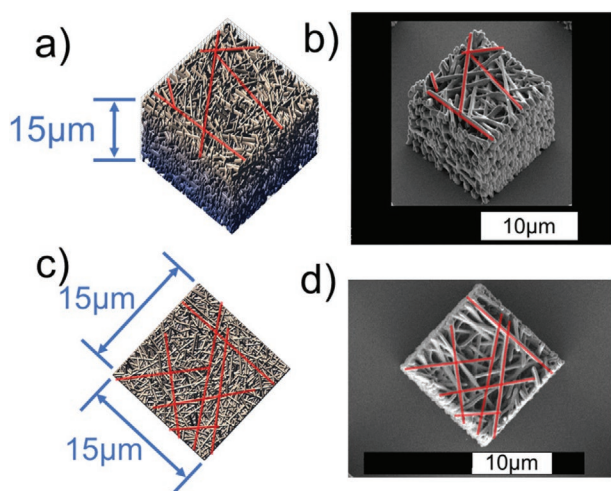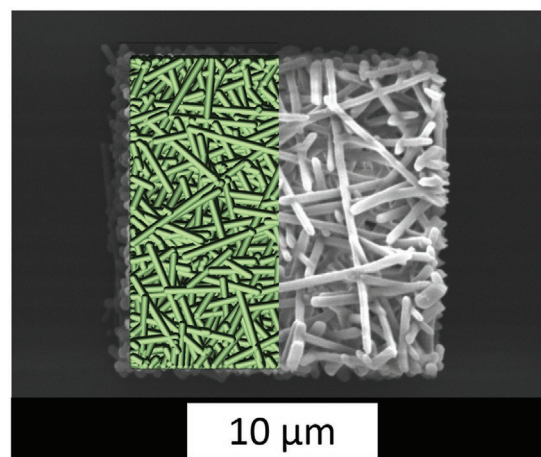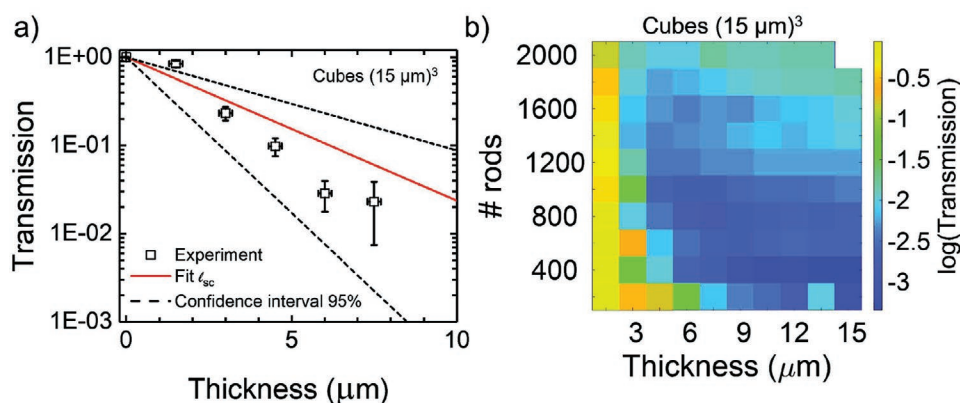
Figure 4. Top view of model and SEM picture of the fabricated structure. One can see that the features evolve continuously between model (shaded in green) and the fabrication (grey SEM image). Some of the smaller rods may not adhere to the main skeleton, but their final contribution is small (≈2 vol%).

The elongated focus of the laser beam in the resist results in an elliptical cross-section of the rods with the semi-major axis along z. The resulting size asymmetry of the voxel is 3.5. We note that the elongation of a rod (i.e., its cross-sectional area) depends on its angle with respect to the z-axis.[27] Although the resemblance between the design and real structure is very good and features remain in the same relative positions as seen in **Figure 4**, there are a few errors in the fabricated structure, for, for example, missing rods and shrinkage artifacts. Typically, the very short rods on the cube faces wash away during development due to insufficient adhesion of these features to the structure. The total number of missing rods is small (few dozen) and their contribution to the structure is very small, estimated to be less than 2 vol% and not easy to discriminate from the final structure as shown in Figure 4. Importantly, these fabrication errors repeat in different realization of the structure, thereby making it feasible to compare their optical interference properties. We did not observe severe pyramidal distortions[36] from the inspection of the SEM images, a distortion that is common in direct laser-written structures.[40,43] Although the residual pyramidal artifacts do decrease the density uniformity, given the modest height of the structures, we expect this effect to have only a small impact on the optical measurements. We conclude that the chosen height and laser dose were a good choice and proceed to the optical characterization of the structures.

3.2. Scattering Characteristics

In order to study the total transmission and extract ℓ_{tr}, we design a set of structures with varying height at a given filling fraction.[7,44] The uniform density of the scatterers certifies an on-average uniform filling fraction also in the structures with a reduced height. The microscopic design of the structures was kept constant and the height of the structures was tuned by writing deeper inside the glass substrate. This avoids

Figure 3. Design of a scattering sample of polymer rods a) in bird's eye view and c) from above. b) and d) SEM images of the fabricated structures according to the designs (a) and (c). We have highlighted several nanorods to ease the comparison of the model and the fabricated sample.

Figure 5. Ballistic light transmission versus thickness for samples with lateral dimension of 15 µm. a) The experimental data are presented with the black markers, while the red solid line shows the fitting to Lambert–Beer law with a scattering mean free path of ℓ_{sc} = 2.6 ± 1.5 µm. The fitting error is 95% confidence interval, shown with the black dashed line. b) The color graph depicts ballistic light transmission for the structures as a function of the rods/volume (x-axis) and thickness (y-axis). The ballistic light attenuates with thickness, as expected. The largest decay of the ballistic light with thickness appears for 400 rods.

the transmission noise that could be introduced by different disorder realizations. In order to study the scattering properties of this design, we fabricated two series of structures with lateral dimensions of 15 and 20 µm. The first series are made of 200 up to 2000 rods per $(15\ \mu m)^3$ with a step size of 200 rods per $(15\ \mu m)^3$, corresponding to a filling fraction from 32 vol% up to 97 vol%. For each filling fraction, we also varied the height from 1.5 µm up to 15 µm with steps of 1.5 µm. The second series is composed of 600 rods per $(20\ \mu m)^3$ up to 2400 rods per $(20\ \mu m)^3$ with a step size of 200 rods per $(20\ \mu m)^3$, corresponding to a filling fraction from 49 vol% up to 93 vol%. For each filling fraction, we also varied the height from 6.5 µm up to 20 µm with a step of 1.5 µm.

Figure 5a shows the physical thickness dependence of the ballistic light transmission in the series of structures with lateral dimensions of 15 µm and 400 inscribed rods. The ballistic transmission decreases exponentially with increasing thickness as $I(\theta = 0, L) = I_0(\theta = 0)\exp(-L/\ell_{sc})$. We used nonlinear least squares fitting of the experimental data and extract $\ell_{sc} = 2.6 \pm 1.5$ µm where the error is the 95% confidence

interval. This value confirms that our media are in the multiple-scattering regime as $L \approx 5 \times \ell_{sc}$.

In the color graph of Figure 5b we summarize the ballistic light measurements for the series with lateral dimensions of 15 µm. On the x-axis, the thickness of the structure increases, while the y-axis shows the number of rods composing the full structures. We observe the sharpest thickness-dependent drop in ballistic light transmission for structures composed of 400 rods, which signifies the shortest ℓ_{sc} among the fabricated structures.

The total transmission measurements are shown in **Figure 6** for structures with edge lengths of 15 µm and 20 µm in Figure 6a and Figure 6b, respectively. The total transmission decreases with increasing thickness of the structure. The two series show a different behavior for increasing thickness, which we attributed to the difference in the scattering mean free path and anisotropy values. The transmission decrease is strongest for structures with 400 rods in Figure 6a and 600 rods in Figure 6b. Referring to Figure 2, we remark that this is at ≈50% filling fraction. This is an interesting contrast compared
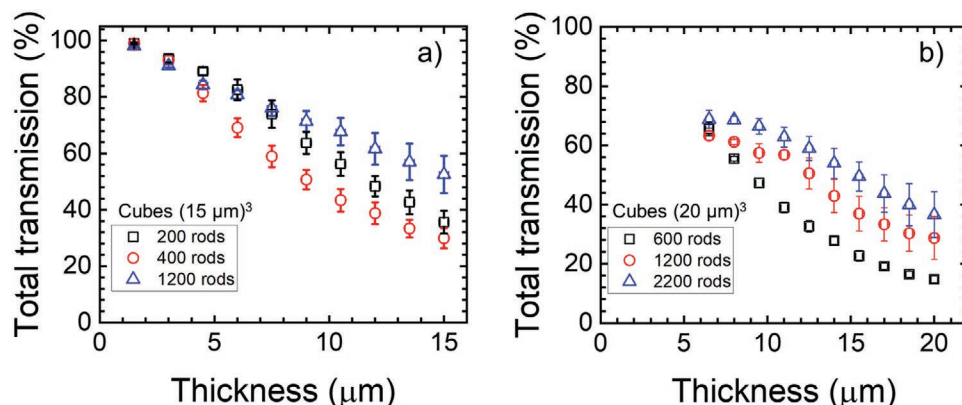
Figure 6. Total transmission of the samples as a function of their thickness. In a) three series of samples are presented with different markers, corresponding to density of rods of 200, 400, and 1200 rods and with lateral dimensions of 15 µm. In b) three more cases are presented, 600, 1200, and 2200 rods and with lateral dimensions of 20 µm. In both cases, the media exhibit strong attenuation of the total transmission that can be tuned with the design parameters.
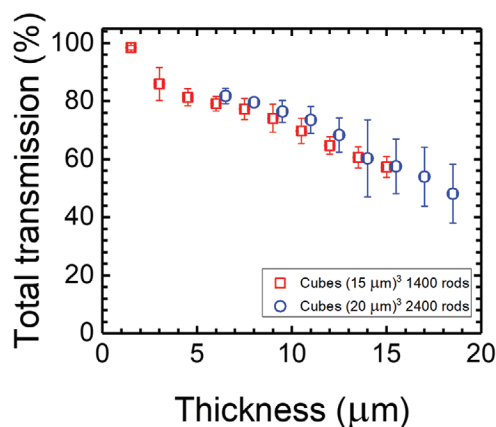
Figure 7. The total transmission values for structures of different density of rods over volume but the same filling fraction. The red markers correspond to experimental measurements series with 1500 rods in a $(15\,\mu m)^3$ cube while the blue markers correspond to series with 2400 rods in a $(20\,\mu m)^3$ cube. The filling fraction for the two series is 93% and both trends match well within error bar, proving consistency in our fabrication and design.

to samples made from spheroidal scatterers that find their maximum photonic strength at smaller values of filling fraction ≈30%. In **Figure 8**, we present the measured total transmission as a function of the filling fraction, for 15 μm and 20 μm lateral dimensions. The lowest total transmission in our media appears at the 400 rods per $(15\,\mu m)^3$ and 600 rods per $(20\,\mu m)^3$, which corresponds to filling fractions of 54% and 49%, respectively. These values of the filling fraction indeed correspond approximately to maximizing the air–polymer interfaces while they are slightly higher than the filling fraction of ≈38% that maximize photonic interaction for systems composed of spherical scatterers.[41,45] To check the consistency of the transmission data for different linked dimensions at identical filling fractions (≈93%), two total transmission series are made: for the 15 μm cubes with 1400 rods and for the 20 μm cubes with 2400 rods. The lateral dimensions and the number of rods in these structures differ, but since the filling fractions coincide, the light

transport is expected to be similar. This consistency is validated from **Figure 7** and highlights that the design method is effective for the chosen finite lateral dimensions and scatterer geometry.

The total transmission T_z for a sample of thickness z, as measured by recording the total power of the light I_z that was transmitted through the structure with given thickness z. The reference power I_0 was measured on a bare glass substrate. The ratio of the total power for given thickness z and the reference I_0 is the total transmission of the sample, $T_z = I_z/I_0$. To extract ℓ_{sc}, the ballistic light attenuation B_z is measured as the ratio $B_z = I_z(\theta = 0)/I_0(\theta = 0)$, where θ is scattering angle with $\theta = 0$ along the propagation direction.

The transport properties of a scattering medium can be derived using the radiative transfer equation, which can be solved analytically only for simple geometries. Given the complexity of the nanofabricated structures that feature substrate reflections and finite size of the structures, it is impossible to exactly solve the radiate transfer equation. Therefore, unambiguous estimation of ℓ_{tr} or g is technically demanding due to the lack of simple-to-use models that can be employed for fitting the measured transmission values. In such a case, several numerical approaches can be used to extract the transport parameters from experimental data.[6,46,47] Light transport Monte Carlo (MC) methods have been successfully employed to numerically solve complex geometries, finite boundary conditions, and even amplifying scattering media.[48,49] We employ MC simulations together with a least-square regression routine to fit the measured total transmission values and robustly extract ℓ_{tr} as described below.

We perform MC simulations that numerically solve the radiate transfer equation[50,51] for our sample geometry assuming an homogeneous distribution of anisotropic scatters in a sample volume as defined by our fabricated sample geometry. Further, we also include Fresnel reflections from the sample substrate in the simulations. Using MC simulations, we compute a look-up table of total transmission values over a wide parameter span of ℓ_{sc} and g. In our computations, the parameter span was set to a range of possible values of ℓ_{sc} and g. For example, we use $\ell_{sc} \in [0.1, 300]\,\mu m$ and $g \in [-1, 1]$. As the
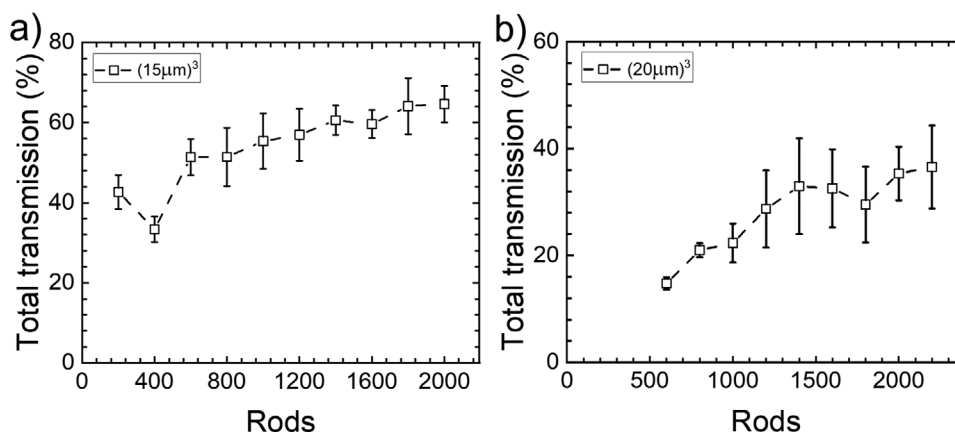
Figure 8. Total transmission of the samples as a function of the density of rods over volume for given thickness. At the plot a), the markers denote the sample size for given volume $(15\,\mu m)^3$ and increasing number of rods. At the plot b), the markers refer to the total transmission measurements versus increasing density of rods over volume for samples of volume $(20\,\mu m)^3$. Both graphs show agreement with Figure 2, where the lower transmission appears for filling fraction of 50%.

2001438 (5 of 7)

ADVANCED
SCIENCE NEWS
www.advancedsciencenews.com

ADVANCED
OPTICAL
MATERIALS
www.advopticalmat.de

total transmission is a smooth function in this 2D parameter space, the computed transmission values could be interpolated on a finer grid as required. Such look-up tables were created for varying sample thicknesses at a given lateral size. The MC estimates together with the measured total transmission data are then used to extract the best fit ℓ_{sc} and g using standard least-squares minimization routine. Note that the value derived here is an approximate value that is characteristic for transport in the z direction averaged over the entire volume. Due to the elongated cross section in the z direction and the overall complexity of the rod network, the anisotropy requires a tensor description.[6,52] Further study of the influence and control of anisotropy in DLW written structures is an intriguing direction for future research.

For a wavelength of 633 nm the MC estimates for the 400 rods yield a scattering mean free path value $\ell_{sc} = 1.8 \pm 0.5$ µm and $g = 0.85 \pm 0.04$, corresponding to $\ell_{tr} = 11.8 \pm 4.5$ µm. For the structure with 600 rods, MC estimates a scattering mean free path $\ell_{sc} = 2.8 \pm 0.3$ µm and $g = 0.65 \pm 0.04$, which corresponds to $\ell_{tr} = 8.3 \pm 1.2$ µm. We summarize the various results in **Table 1**. Comparing the results leads to a few observations: The 400 rods structure yields a smaller ℓ_{sc} compared to the 600 rods structure. However, due to their respective value for the anisotropies, the corresponding order for their ℓ_{tr} is inverted. We theorize that this occurs because at a higher density of rods we obtain a smaller value of the anisotropy. The more rods per volume, the less pronounced their geometrical features are, resulting in washing out the high anisotropy values. Vice versa this means that the scattering mean free path together with the anisotropy can be used to influence the transport mean free path. For us, the most important conclusion is that the DLW structures are diffusive since their thickness surpasses the transport mean free path $L > \ell_{tr}$, while possessing µm range ℓ_{sc} and large g.

4. Conclusion

We have implemented a DLW method to fabricate small deterministic optical multiple scattering media with optical thickness $\frac{L}{\ell_{tr}} > 1$. The fabrication process allows full control over the position and shape of the scatterers. We show that one can tune the density of scatterers and accordingly vary the transport mean free path. We demonstrate that our best design has a scattering mean free path of $\ell_{sc} = 1.8 \pm 0.5$ µm. The deterministic nature of fabrication opens up the possibility for new fundamental studies of light propagation in scattering media. This permits validation of various fundamental and applied aspects

of light scattering for a given disordered structure, something that was not possible until now for optical frequencies.[53] In the future, we want to investigate the reproducibility of the method to study the clonability of multiple scattering media as optical physical unclonable functions.[54]

5. Experimental Section

Direct Laser Writing: The structures were fabricated with a direct laser writing system[27] (Nanoscribe Professional GT, using polymer photoresist Nanoscribe IP-G with a refractive index of 1.51 for a wavelength of 633 nm[55]). The photoresist is a gel and its high viscosity ensured that the features in the structures did not drift during the writing processes, thereby minimizing deformation of the structures. The illumination dose was set to be 14% higher than the polymerization threshold (laser beam power 8.90 mW and piezomotors scan speed of 140 µm s^{-1}). This higher dose resulted in rods of an average thickness of 500 nm instead of 100 nm that one could reach with a smaller illumination dose. Although the choice of a dose closer to the polymerization threshold would provide finer features,[56] the slightly higher dose provided two advantages in the nanofabrication of those media. Firstly, thicker rods provided more robust mechanical support of the structure without any additional walls, thereby enabling self-supported structures unlike earlier demonstrations.[57] The second advantage of a higher dose was the reduction of fabrication disorder through the complete cross-linking of polymer chains across the entire volume.[58]

Optical Setup: The optical scattering strength in the samples is quantified by extracting the transport mean free path ℓ_{tr} using total transmission measurements.[7] The experimental setup is shown in **Figure 9**. The laser beam from a linearly polarized He–Ne laser ($\lambda = 633$ nm, beam diameter of 3 mm) was expanded 10× with a beam expander and focused with a plano-convex lens (focal length = +100 mm) onto the sample. The focused beam had a full-width at half-maximum of 4 µm, smaller than the lateral dimensions of 15 and 20 µm of the structures. An oil-immersion objective (numerical aperture NA = 1.4) was used to collect the light transmitted light through the photonic scattering medium. Each structure was positioned with a 3-axis piezo positioning stage, while viewing with a
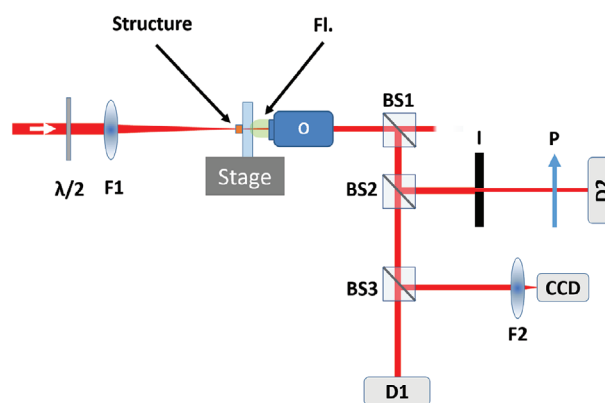
Figure 9. Schematic of the set up for measuring the total transmission and ballistic light attenuation. a) A continuous wave He:Ne laser at 633 nm is expanded to a diameter of 3.1 cm and focused on a single structure with an aspheric lens F1 with a focal length of 100 mm. A microscope oil immersion (Fl.) objective with NA = 1.4 collects the transmitted light from the glass surface. Illumination of a specific structure is controlled with the use of a 3-axis piezo positioning stage. We use a CCD camera to confirm correct positioning while the total transmission is recorded with a power meter (D1). The light that is reflected by BS2 is used to evaluate the ballistic light attenuation. An iris with a polarizer aligned parallel to the polarization of the laser beam filters out the scattered light. The filtered light intensity is measured with a power meter (D2).

Table 1. Transport parameters estimated by fitting the measured total transmission with the Monte Carlo simulations. Apart from the scattering mean free path ℓ_{sc}, the anisotropy g and the transport mean free path ℓ_{tr}, also the optical thickness L_{opt} is listed.

Parameter	400 rods per (15 µm)^3	600 rods per (20 µm)^3
ℓ_{sc}	1.8 ± 0.5 µm	2.8 ± 0.3 µm
g	0.85 ± 0.04	0.65 ± 0.04
ℓ_{tr}	12 ± 4 µm	8 ± 1 µm
L_{opt}	1.2 ± 0.3	2.5 ± 0.1

CCD camera. The light collected by the objective was split with three non-polarizing 50:50 beam splitters (BS1–3). The transmitted part of BS3 was sent to power meter(D1) to obtain the total transmission. The reflected part of BS2 was used to monitor the ballistic light. For this reason, it was filtered with an adjustable iris. A polarizer filtered out multiple-scattered light, allowing only polarization components parallel to the original beam polarization to be transmitted to the power meter (D2).

Conflict of Interest

The authors declare no conflict of interest.

[1] J. W. Goodman, *J. Opt. Soc. Am.* **1976**, *66*, 1145.
[2] A. Ishimaru, *Wave Propagation and Scattering in Random Media*, Vol. 2, Academic Press, New York **1978**.
[3] M. P. van Albada, A. Lagendijk, *Phys. Rev. Lett.* **1985**, *55*, 2692.
[4] P.-E. Wolf, G. Maret, *Phys. Rev. Lett.* **1985**, *55*, 2696.
[5] A. Z. Genack, *Phys. Rev. Lett.* **1987**, *58*, 2043.
[6] W.-F. Cheong, S. A. Prahl, A. J. Welch, *IEEE J. Quantum Electron.* **1990**, *26*, 2166.
[7] N. Garcia, A. Z. Genack, A. A. Lisyansky, *Phys. Rev. B* **1992**, *46*, 14475.
[8] M. I. Mishchenko, *Appl. Opt.* **1993**, *32*, 4652.
[9] A. Lagendijk, B. A. Van Tiggelen, *Phys. Rep.* **1996**, *270*, 143.
[10] M. C. W. van Rossum, T. M. Nieuwenhuizen, *Rev. Mod. Phys.* **1999**, *71*, 313.
[11] E. Akkermans, G. Montambaux, *Mesoscopic Physics of Electrons and Photons*, Cambridge University Press, Cambridge, UK **2007**.
[12] D. S. Wiersma, *Nat. Photonics* **2013**, *7*, 188.
[13] W. L. Vos, T. W. Tukker, A. P. Mosk, A. Lagendijk, W. L. IJzerman, *Appl. Opt.* **2013**, *52*, 2602.
[14] M. Burresi, F. Pratesi, K. Vynck, M. Prasciolu, M. Tormen, D. S. Wiersma, *Opt. Express* **2013**, *21*, A268.
[15] S. Rotter, S. Gigan, *Rev. Mod. Phys.* **2017**, *89*, 015005.
[16] M. L. Meretska, R. Uppu, G. Vissenberg, A. Lagendijk, W. L. IJzerman, W. L. Vos, *Opt. Express* **2017**, *25*, A906.
[17] G. Jacucci, J. Bertolotti, S. Vignolini, *Adv. Optical Mater.* **2019**, *7*, 1900980.
[18] N. Garcia, A. Z. Genack, *Phys. Rev. Lett.* **1989**, *63*, 1678.
[19] H. Cao, Y. G. Zhao, H. C. Ong, S.-T. Ho, J. Y. Dai, J. Y. Wu, R. P. H. Chang, *Appl. Phys. Lett.* **1998**, *73*, 3656.
[20] F. J. P. Schuurmans, D. Vanmaekelbergh, J. van de Lagemaat, A. Lagendijk, *Science* **1999**, *284*, 141.
[21] F. J. P. Schuurmans, M. Megens, D. Vanmaekelbergh, A. Lagendijk, *Phys. Rev. Lett.* **1999**, *83*, 2183.
[22] P. D. García, R. Sapienza, C. López, *Adv. Mater.* **2010**, *22*, 12.
[23] J. M. Miranda-Muñoz, G. Lozano, H. Míguez, *Adv. Optical Mater.* **2017**, *5*, 1700025.
[24] S. Molesky, Z. Lin, A. Y. Piggott, W. Jin, J. Vucković, A. W. Rodriguez, *Nat. Photonics* **2018**, *12*, 659.
[25] R. E. Christiansen, F. Wang, O. Sigmund, *Phys. Rev. Lett.* **2019**, *122*, 234502.
[26] M. Farsari, M. Vamvakaki, B. N. Chichkov, *J. Opt.* **2010**, *12*, 124001.
[27] J. Fischer, M. Wegener, *Laser Photon. Rev.* **2013**, *7*, 22.
[28] G. Seniutinas, A. Weber, C. Padeste, I. Sakellari, M. Farsari, C. David, *Microelectron. Eng.* **2018**, *191*, 25.
[29] F. Utel, L. Cortese, D. S. Wiersma, L. Pattelli, *Adv. Optical Mater.* **2019**, *7*, 1900043.
[30] O. Matoba, Y. Kitamura, T. Manabe, K. Nitta, W. Watanabe, *Appl. Phys. Lett.* **2009**, *95*, 221114.
[31] R. R. Gattass, E. Mazur, *Nat. Photonics* **2008**, *2*, 219.
[32] D. Di Battista, D. Ancora, H. Zhang, K. Lemonaki, E. Marakis, E. Liapis, S. Tzortzakis, G. Zacharakis, *Optica* **2016**, *3*, 1237.
[33] M. Thiel, J. Fischer, G. von Freymann, M. Wegener, *Appl. Phys. Lett.* **2010**, *22*, 10.
[34] M. T. Do, T. T. N. Nguyen, Q. Li, I. Ledoux-Rak, N. D. Lai, *Opt. Express* **2013**, *21*, 20964.
[35] P. Kiefer, V. Hahn, M. Nardi, L. Yang, E. Blasco, C. Barner-Kowollik, M. Wegener, *Adv. Optical Mater.* **2020**, 2000895.
[36] J. Haberko, N. Muller, F. Scheffold, *Phys. Rev. A* **2013**, *88*, 043822.
[37] J. Haberko, F. Scheffold, *Opt. Express* **2013**, *21*, 1057.
[38] N. Muller, J. Haberko, C. Marichy, F. Scheffold, *Adv. Optical Mater.* **2014**, *2*, 115.
[39] E. Marakis, M. C. Velsink, L. J. C. van Willenswaard, R. Uppu, P. W. H. Pinkse, *Phys. Rev. E* **2019**, *99*, 043309.
[40] H.-B. Sun, S. Kawata, *Two-Photon Photopolymerization and 3D Lithographic Microfabrication*, Springer, Berlin, Heidelberg **2004**, pp. 169–273.
[41] W. L. Vos, H. M. van Driel, M. Megens, A. F. Koenderink, A. Imhof, In *Photonic Crystals and Light Localization in the 21st Century*, Springer, Dordrecht, The Netherlands **2001**, pp. 191–218.
[42] X. Zhou, Y. Hou, J. Lin, *AIP Adv.* **2015**, *5*, 030701.
[43] A. A. Bauhofer, S. Krödel, J. Rys, O. R. Bilal, A. Constantinescu, C. Daraio, *Adv. Mater.* **2017**, *29*, 1703024.
[44] M. B. van der Mark, M. P. van Albada, A. Lagendijk, *Phys. Rev. B* **1988**, *37*, 3575.
[45] K. Busch, C. M. Soukoulis, E. N. Economou, *Phys. Rev. B* **1994**, *50*, 93.
[46] H. C. Van de Hulst, *Multiple Light Scattering: Tables, Formulas, and Applications*, Elsevier, New York **2012**.
[47] L. Yang, B. Kruse, *J. Opt. Soc. Am. A* **2004**, *21*, 1933.
[48] S. A. Prahl, M. Keijzer, S. L. Jacques, A. J. Welch, in *Dosimetry of Laser Radiation in Medicine and Biology*, Proc. SPIE Vol. 10305, International Society for Optics and Photonics, Washington DC **1989**, p. 1030509.
[49] R. Uppu, S. Mujumdar, *Phys. Rev. Lett.* **2015**, *114*, 183903.
[50] R. Uppu, S. Mujumdar, *Phys. Rev. A* **2013**, *87*, 013822.
[51] M. L. Meretska, *Ph.D. Thesis*, University of Twente, **2018**.
[52] R. Sapienza, S. Mujumdar, C. Cheung, A. G. Yodh, D. Wiersma, *Phys. Rev. Lett* **2004**, *92*, 033903.
[53] W. Choi, A. P. Mosk, Q.-H. Park, W. Choi, *Phys. Rev. B* **2011**, *83*, 134207.
[54] S. A. Goorden, M. Horstmann, A. P. Mosk, B. Škorić, P. W. H. Pinkse, *Optica* **2014**, *1*, 421.
[55] T. Gissibl, S. Wagner, J. Sykora, M. Schmid, H. Giessen, *Opt. Mater. Express* **2017**, *7*, 2293.
[56] M. G. Guney, G. K. Fedder, *J. Micromech. Microeng.* **2016**, *26*, 105011.
[57] M. Deubel, G. Von Freymann, M. Wegener, S. Pereira, K. Busch, C. M. Soukoulis, *Nat. Mater.* **2004**, *3*, 444.
[58] K.-S. Lee, R. H. Kim, D.-Y. Yang, S. H. Park, *Prog. Polym. Sci.* **2008**, *33*, 631.